MONOLITHIC ELECTROWETTING PRISM FOR STRUCTURED ILLUMINATION MICROSCOPY

Eduardo J. Miscles[1], Catherine A. Saladrigas[1], Mo Zohrabi[1], Vikrant Kumar[2], Ioannis Kymissis[2], Juliet T. Gopinath[1], and Victor M. Bright[1]*
[1]University of Colorado, Boulder, Colorado, USA
[2]Columbia University, New York, New York, USA

ABSTRACT

We demonstrate MEMS electrowetting-based tunable prism fabrication advancements and integrate a device as a scanning element in structured illumination microscopy system. The successful development of a monolithic electrowetting prism with a 30 µm electrode gap on a vertical sidewall was achieved using direct laser write lithography on three-dimensional, high aspect ratio curved glass substrates. The device exhibits significantly improved imaging performance compared to devices fabricated with other methods, as demonstrated by a four-fold increase in contrast when imaging a microLED display. This improvement enables a novel implementation of optical sectioning structured illumination microscopy.

KEYWORDS

Electrowetting, adaptive optics, liquid lens, optical device, liquid prism, tunable liquid device, direct laser write lithography, structured illumination microscopy.

INTRODUCTION

Light steering technologies are necessary for various optical systems ranging from scanning microscopy [1, 2] to optical displays [3, 4]. Depending on the application, the scanning element can be mechanical such as microelectromechanical systems (MEMS) mirrors [5–7] and galvanometric mirrors [8, 9], or non-mechanical such as spatial light modulators [10, 11], and liquid crystals [12, 13]. Although a multitude of scanning technologies are available, the choices become limited when size, weight and power constrained environments are considered. In these cases, one attractive solution is electrowetting tunable optics. These optics stand out for their mechanical simplicity, compactness, low-power operation, high-speed capabilities, and transmissive nature. Electrowetting prisms have already shown promise for LiDAR [14–16], laser scanning microscopy [8], solar tracking [17], and wavefront control [18–20].

Here, we report on fabrication of monolithic electrowetting tunable prisms exhibiting individually addressable sidewall electrodes with a separation of 30 µm. The small electrode gap enables the use of electrowetting prisms that have minimal aberrations in an imaging demonstration. We demonstrate the devices in a novel implementation of optical sectioning structured illumination microscopy (OS-SIM), enhancing the axial resolution of a standard epifluorescence microscope.

Electrowetting Background

Electrowetting-on-dielectric involves applying an electric field to modify the wetting properties of a solid surface. This process changes the contact angle of a polar liquid droplet by applying voltage across the droplet and an electrode separated by a dielectric layer [21–25]. The Lippmann-Young equation determines the contact angle based on applied voltage, V,

$$\cos(\theta) = \cos(\theta_0) + \eta V^2 \quad (1)$$

where θ is the contact angle, θ_0 is the zero voltage contact angle, and η is a constant dependent on material properties.

We leverage this effect by functionalizing cylindrical glass tubes with an electrode layer, a dielectric layer, and a hydrophobic layer (used to increase the initial contact angle). The functionalized glass tubes are attached to a bottom optical ground window and filled with immiscible polar and non-polar liquids of contrasting refractive indices. We use deionized (DI) water as the polar liquid and 1-phenyl-1-cyclohexene (PCH) as the non-polar liquid, selected for their large refractive index contrast ($\Delta n = 0.17$), fast actuation speeds, and minimum density mismatch ($\Delta\rho < 0.01\ g/L$) [26–28]. We further increase control over the liquid interface by including multiple, individually addressable sidewall electrodes. In this case, the electrowetting-controlled liquid-solid contact angle is localized at the electrode, resulting in the ability to actuate the liquid interface in an asymmetric manner. For example, when all four electrodes are biased to V_{flat} (the voltage corresponding to a 90° contact angle), a voltage differential, V_{scan}, can be applied to opposing electrodes, such that $V_1 = V_{flat} - V_{scan}$ and $V_2 = V_{flat} + V_{scan}$, resulting in $\theta_1 > \theta_2$, a representative schematic of this scenario is shown in Fig. 1. The liquid-solid contact angle at the electrode gap remains as θ_0, as there is no voltage applied in the gap. This discontinuity in the contact angle leads to poor optical quality surfaces if the gap is too large, a challenge we seek to address in this work.

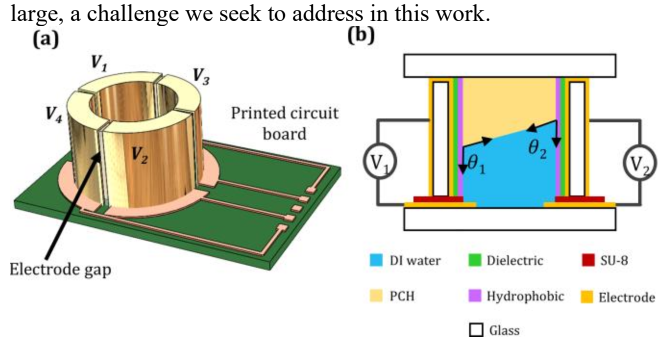

Figure 1: (a) A perspective view of the four-electrode prism device, with the electrodes labelled with V_1 through V_4 and the electrode gap separation. (b) Cross-sectional image of an electrowetting prism showing voltage application on the vertical electrode and bottom ground electrode. At the voltage V_{flat}, the contact angle of the liquid interface with the device wall is 90°. A voltage differential V_{scan} applied to opposing electrodes results in a tilted liquid interface.

DEVICE FABRICATION

Previously, monolithic electrowetting based tunable prisms have been fabricated in cylindrical containers at millimeter scale using Kapton tape [29] or 3D printed masks [26] to pattern the electrode gap on the sidewall. While these methods are reliable, they suffer from large electrode separations, ~1 mm in the case of Kapton masks, and ~400 µm in the case of 3D printed shadow masks. Non-cylindrical designs have also been demonstrated by fabricating planar substrates which are then assembled into rectangular containers [15], but the sharp corners and rectangular geometry that result from this method lead to poor optical surfaces. Other designs such as that by Kopp *et al.* have demonstrated high quality optical surfaces by using 2D lithography to fabricate addressing electrodes on polyimide substrates which are then rolled and inserted into cylindrical glass tubes [20]. While this leads to high optical quality surfaces, the multi-piece design can make device packaging difficult compared with a monolithic layout. In this work, we present a method for fabricating monolithic four electrode electrowetting prisms in cylindrical containers with an order of magnitude smaller electrode gap size compared to Kapton or 3D printed masks, allowing for OS-SIM imaging using our devices.

Direct Write Lithography System

One of the most prevalent lithography methods is contact lithography [30], wherein a pattern is exposed onto photoresists using a mask. Although highly repeatable and fast, this method is not well-suited for non-planar substrates. One alternative for writing photoresist patterns is direct laser write lithography, where a laser source scans across the photoresist. This method offers higher resolution limits, determined by the objective used and wavelength of the laser source [31]. A simple, cost-effective approach for achieving direct laser write lithography for SU-8 patterning involves using commercially available 405 nm laser diodes and motorized stages to scan either the light source or the substrate [31, 32].

Here, we present a direct-write lithography system capable of patterning photoresist on three-dimensional substrates. The system employs a 405 nm laser diode collimated to ~1 mm full width at half maximum (FWHM) diameter and focused through a 10X, 0.28 numerical aperture (NA), long working distance objective (Mitutoyo Plan Apo). Figure 2(a) illustrates the exposure system configured to focus UV light on the inner tube wall of an SU-8 coated glass tube. Utilizing a motorized stage, we scan the coated tube vertically, followed by a 90° rotation and repetition of the process. This results in developed ~30 µm wide sections of SU-8 spanning the tube's 5 mm height. Figure 2(b) shows the processed and developed SU-8 on the inner wall of a glass tube. This SU-8 section serves as a mask when the tube is sputter-coated with the electrode material, and an SU-8 lift-off process is executed to create the functionalized glass tube, as detailed in the fabrication section.

Electrowetting Prism Fabrication

We start by cleaning a 4 mm inner diameter, 5 mm tall glass tube with acetone and isopropyl alcohol, followed by drying with compressed nitrogen. A layer of SU-8 3010 is then coated on the inner sidewall using a polyurethane foam swab and soft baked at 65°C for 5 minutes.

Next, the SU-8 is exposed using the custom-built laser lithography system described above. The SU-8 coated inner sidewall of the tube is placed at the focal spot of the objective, and a motorized stage is used to move the tube vertically at 100 µm/s, resulting in an exposure dosage of 980 J/cm^2. After rotating the tube 90°, the exposure process is repeated three more times. A post-exposure bake at 95°C for 6 minutes follows, and then the SU-8 is submerged in developer for 5 minutes.

The adhesion of SU-8 near the tube rim was found to be inconsistent, and a mask for the outside of the glass tube must be made to maintain electrical isolation of the electrodes. To solve both issues, a single 3D printed shadow mask spanning the tube's height at the outer diameter and protruding 500 µm inside at the top and bottom is used, as shown in Fig. 2(c). Indium tin oxide (ITO) is uniformly deposited using direct current sputtering at 60 W and 15 mTorr argon pressure. The shadow mask is removed, and an SU-8 lift-off is performed.

Following this, the tubes are rinsed with isopropyl alcohol, and the conductivity of the ITO electrodes is enhanced by annealing at 300°C for one hour. Before applying dielectric and hydrophobic layers, the outer diameter is masked with Kapton tape. Parylene HT (3 µm) is vapor-phase deposited, followed by dip-coating in a 10 wt.% Cytop solution and curing at 185°C for one hour.

An optical ground window is fabricated on a glass substrate by lithographically patterning annular electrodes using NR-7 photoresist. A ground electrode of 50 nm Ti/300 nm Au is sputtered, and excess material is removed through lift-off in acetone. SU-8 3050 (50 µm) is deposited and patterned as an electrical insulation layer.

The functionalized glass tube is aligned and epoxy bonded to the ground window, and a custom printed circuit board is attached with silver epoxy for electrical connection to driving electronics.

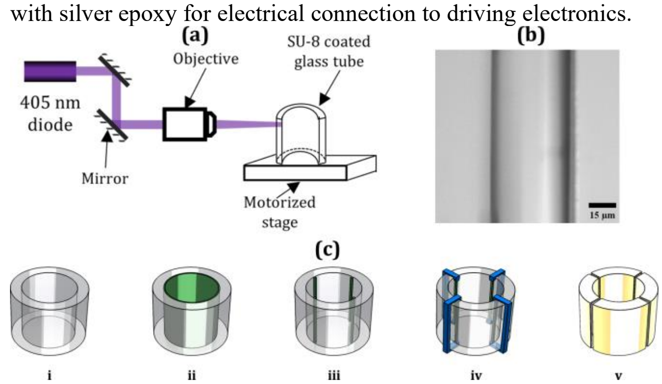

Figure 2: (a) Diagram of the laser lithography system. (b) Optical microscope image of an exposed and developed layer of SU-8 on the inner sidewall of a cylindrical glass tube. (c) Fabrication process for electrowetting prisms: i) Prepare a clean glass tube. ii) Coat inner sidewall with SU-8. iii) Pattern and develop SU-8. iv) Install shadow mask on tube to mask outer sidewall and inner tube edges. v) Sputter deposit electrode and perform SU-8 lift-off.

EXPERIMENTAL METHODS AND RESULTS

We use our devices to enhance optical sectioning structured illumination microscopy (OS-SIM), a widefield imaging technique using sinusoidal illumination patterns. This technique requires imaging three distinct spatial phases of the illumination pattern on the sample in order to reconstruct an optically sectioned image [33]. We use a striped microLED array which has been demonstrated as an illumination source for OS-SIM [34]. The benefit of including an electrowetting tunable prism is the ability to load a static pattern on the display which is then shifted in the imaging plane by tuning the prism angle, allowing fine control over the phase of the illumination.

To preserve the imaged pattern, the distortions of the liquid interface caused by the electrode gap must be sufficiently small. To illustrate, we use a standard epifluorescence microscope with a patternable microLED display as the 455 nm excitation source. Following the display, the electrowetting tunable prism is inserted and the electrodes are actuated to a 90° liquid interface contact angle. The microLED pattern is imaged through the actuated device on the sample plane with a tube lens (Olympus SWTLU-C) and objective (20X, 0.42 NA, Mitutoyo Plan Apo). The objective is on a piezo stage, enabling axial scanning through a sample. The fluorescence from the sample is collected back through the objective and tube lens and reflected by a short pass dichroic onto a CMOS sensor, as shown in Fig. 3. Comparisons between a 400 µm and 30 µm electrode gap electrowetting prisms are made by imaging a 40 µm period illumination pattern on to a fluorescent target. Fluorescence images shown in Fig. 4(a) and (b) reveal a significant improvement in the imaged pattern with the 30 µm gap device. We quantify this enhancement by comparing the intensity contrast (c) of the peaks (I_{max}) and nulls (I_{min}) of the illumination pattern, defined as

$$c = (I_{max} - I_{min})/(I_{max} + I_{min}) \quad (2).$$

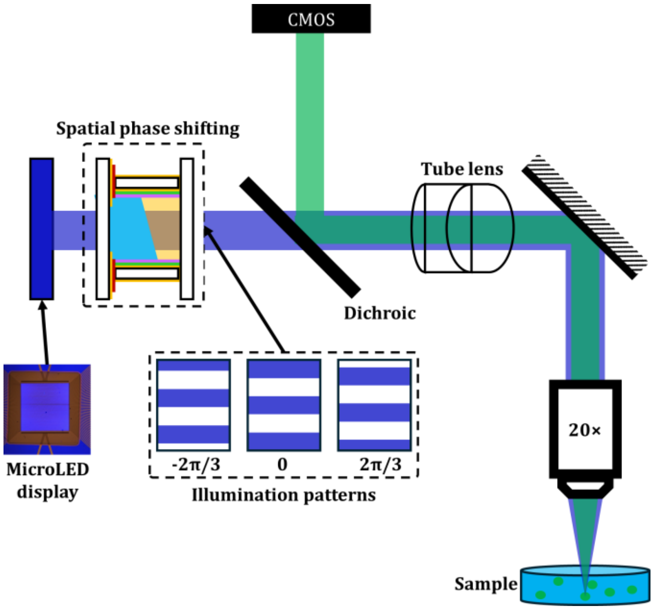

Figure 3: Diagram of an epifluorescence microscope with OS-SIM capability. A microLED display serves as the excitation source, while an electrowetting prism spatially shifts the loaded pattern. Fluorescence from the sample is collected through the objective and tube lens, then reflected onto a CMOS sensor by a short pass dichroic.

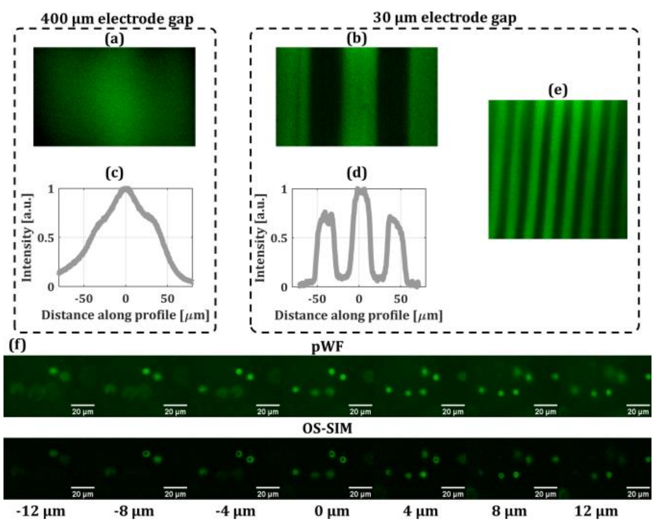

Figure 4: (a- b) Images of 40 µm pitch pattern on thin fluorescent sample when transmitted through an electrowetting prism when all electrodes are actuated to 90º contact angle. The images correspond to a 400 and 30 µm electrode gap device, respectively. (c) Average intensity profile of the pattern when transmitted through a 400 µm electrode gap device. (d) Average intensity profile of the pattern when transmitted through a 30 µm electrode gap device. (e) Image of 12 µm pitch pattern on thin fluorescent sample when transmitted through a 30 µm electrode gap device. (f) Comparison between pWF (top) and OS-SIM (bottom) for a z-stack taken through a tissue phantom.

From the average intensity profiles shown in Fig. 4(c) and (d) we find 85% contrast for the 30 µm gap device, a substantial improvement compared to the 19% contrast achieved by the 400 µm gap device. This enhancement is critical for creating an optical sectioning microscope. The result is increased axial resolution, achieved with an electrowetting tunable prism combined with a microLED display in an epifluorescence microscope.

We demonstrate the optical sectioning capability of the benchtop microscope by imaging a tissue phantom. The phantom is prepared by suspending 1 and 5 µm fluorescent beads in an agarose gel, which mimics scattering properties of tissue. The microLED array displays a pattern which corresponds to a 12 µm period in the sample plane, as shown in Fig. 4(e). At each axial step we take three images: one with the electrowetting device actuated to flat with no voltage differential (0 phase shift), and two more with a 0.25 and -0.25 V differential applied to opposing electrodes, corresponding to $\pm 2\pi/3$ phase shifts of the pattern. The reconstruction is performed using the standard algorithm for OS-SIM [35]. Non-sectioned images are obtained by averaging the three images together, referred to as the pseudo widefield (pWF) image. In Fig. 4(f) we show both the pWF and the OS-SIM images at varying depths into the tissue phantom, demonstrating the strength of the optical sectioning. The artifacts from out of focus beads are clearly removed in the OS-SIM images, and the increased axial resolution allows us to isolate optical sections of the sample.

CONCLUSIONS

In summary, this work has successfully demonstrated the fabrication of a monolithic electrowetting prism with 30 µm electrode gaps, and its subsequent implementation for OS-SIM. The key innovation lies in minimizing the electrode gap to enhance optical performance, a crucial factor for applications in microscopy. Through experimental validation, we have shown that a 30 µm electrode gap on a 4 mm inner diameter device provides the necessary optical quality liquid-liquid interface for imaging fine spatial frequency displays, allowing us to implement our devices to enhance OS-SIM applications. This advancement positions electrowetting optics as promising components for compact and efficient optical systems. The small footprint, simplicity, and enhanced imaging quality make electrowetting prisms a compelling choice for future developments in optical scanning technologies.

ACKNOWLEDGEMENTS

The authors acknowledge the use of Colorado Shared Instrumentation in Nanofabrication and Characterization (COSINC) and JILA fabrication facilities at the University of Colorado Boulder. Funding provided by National Institutes of Health (R01NS118188, UF1NS116241, R01NS123665), Office of Naval Research (N00014-20-1-2087) and National Science Foundation (1926668, 1926676).

REFERENCES

[1] F. Helmchen and W. Denk, "Deep tissue two-photon microscopy," *Nat. Methods*, vol. 2, no. 12, pp. 932–940, Dec. 2005.

[2] W. J. Alford, R. D. VanderNeut, and V. J. Zaleckas, "Laser scanning microscopy," *Proc. IEEE*, vol. 70, no. 6, pp. 641–651, 1982.

[3] M.-H. Kiang, O. Solgaard, K. Y. Lau, and R. S. Muller, "Polysilicon optical microscanners for laser scanning displays," *Sens. Actuators Phys.*, vol. 70, no. 1–2, pp. 195–199, Oct. 1998.

[4] J. Bae, Y.-S. Choi, K. Choi, Y. Kim, Y. Kwon, H. Song, E. Kim, S. Choi, J. Lee, and S. Lee, "Arrayed beam steering device for advanced 3D displays," presented at the SPIE MOEMS-MEMS, San Francisco, California, USA, 2013, p. 86160H.

[5] C. Zhao, Y. Zhu, D. Zhang, Q. Fu, M. Pan, R. Wu, A. Wang, and H. Cheng, “Millimeter field-of-view miniature two-photon microscopy for brain imaging in freely moving mice,” *Opt. Express*, vol. 31, no. 20, p. 32925, Sep. 2023.

[6] W. Zong, H. A. Obenhaus, E. R. Skytøen, H. Eneqvist, N. L. De Jong, R. Vale, M. R. Jorge, M.-B. Moser, and E. I. Moser, “Large-scale two-photon calcium imaging in freely moving mice,” *Cell*, vol. 185, no. 7, pp. 1240-1256.e30, Mar. 2022.

[7] W. Piyawattanametha, E. D. Cocker, L. D. Burns, R. P. J. Barretto, J. C. Jung, H. Ra, O. Solgaard, and M. J. Schnitzer, “In vivo brain imaging using a portable 29 g two-photon microscope based on a microelectromechanical systems scanning mirror,” *Opt. Lett.*, vol. 34, no. 15, p. 2309, Aug. 2009.

[8] O. D. Supekar, B. N. Ozbay, M. Zohrabi, P. D. Nystrom, G. L. Futia, D. Restrepo, E. A. Gibson, J. T. Gopinath, and V. M. Bright, “Two-photon laser scanning microscopy with electrowetting-based prism scanning,” *Biomed. Opt. Express*, vol. 8, no. 12, p. 5412, Dec. 2017.

[9] B. Jaeggi, B. Neuenschwander, U. Hunziker, J. Zuercher, T. Meier, M. Zimmermann, K. H. Selbmann, and G. Hennig, “Ultra-high-precision surface structuring by synchronizing a galvo scanner with an ultra-short-pulsed laser system in MOPA arrangement,” presented at the SPIE LASE, San Francisco, California, USA, 2012, p. 82430K.

[10] E. Haellstig, J. Stigwall, M. Lindgren, and L. Sjoqvist, “Laser beam steering and tracking using a liquid crystal spatial light modulator,” presented at the AeroSense 2003, Orlando, FL, 2003, p. 13.

[11] Q. Niu and C. Wang, “High precision beam steering using a liquid crystal spatial light modulator,” *Opt. Quantum Electron.*, vol. 51, no. 6, p. 180, Jun. 2019.

[12] Z. He, F. Gou, R. Chen, K. Yin, T. Zhan, and S.-T. Wu, “Liquid Crystal Beam Steering Devices: Principles, Recent Advances, and Future Developments,” *Crystals*, vol. 9, no. 6, p. 292, Jun. 2019.

[13] D. P. Resler, D. S. Hobbs, R. C. Sharp, L. J. Friedman, and T. A. Dorschner, “High-efficiency liquid-crystal optical phased-array beam steering,” *Opt. Lett.*, vol. 21, no. 9, p. 689, May 1996.

[14] M. Zohrabi, W. Y. Lim, R. H. Cormack, O. D. Supekar, V. M. Bright, and J. T. Gopinath, “Lidar system with nonmechanical electrowetting-based wide-angle beam steering,” *Opt. Express*, vol. 27, no. 4, p. 4404, Feb. 2019.

[15] J. Lee, J. Lee, and Y. H. Won, “Beam steering and forming in compact electrowetting prism array with separate electrode control,” *OSA Contin.*, vol. 4, no. 9, p. 2400, Sep. 2021.

[16] N. R. Smith, D. C. Abeysinghe, J. W. Haus, and J. Heikenfeld, “Agile wide-angle beam steering with electrowetting microprisms,” *Opt. Express*, vol. 14, no. 14, p. 6557, 2006.

[17] J. Cheng, S. Park, and C.-L. Chen, “Optofluidic solar concentrators using electrowetting tracking: Concept, design, and characterization,” *Sol. Energy*, vol. 89, pp. 152–161, Mar. 2013.

[18] M. Zohrabi, R. H. Cormack, C. Mccullough, O. D. Supekar, E. A. Gibson, V. M. Bright, and J. T. Gopinath, “Numerical analysis of wavefront aberration correction using multielectrode electrowetting-based devices,” *Opt. Express*, vol. 25, no. 25, p. 31451, Dec. 2017.

[19] P. Zhao, D. Sauter, and H. Zappe, “Tunable fluidic lens with a dynamic high-order aberration control,” *Appl. Opt.*, vol. 60, no. 18, p. 5302, Jun. 2021.

[20] D. Kopp and H. Zappe, “Tubular astigmatism-tunable fluidic lens,” *Opt. Lett.*, vol. 41, no. 12, p. 2735, Jun. 2016.

[21] B. Berge and J. Peseux, “Variable focal lens controlled by an external voltage: An application of electrowetting,” *Eur. Phys. J. E*, vol. 3, no. 2, pp. 159–163, Oct. 2000.

[22] F. Mugele and J.-C. Baret, “Electrowetting: from basics to applications,” *J. Phys. Condens. Matter*, vol. 17, no. 28, pp. R705–R774, Jul. 2005.

[23] B. H. W. Hendriks, S. Kuiper, M. A. J. VAN As, C. A. Renders, and T. W. Tukker, “Electrowetting-Based Variable-Focus Lens for Miniature Systems,” *Opt. Rev.*, vol. 12, no. 3, pp. 255–259, May 2005.

[24] H. Ren and S. Wu, *Introduction to Adaptive Lenses*, 1st ed. Wiley, 2012.

[25] J.-C. Baret, M. M. J. Decré, and F. Mugele, “Self-Excited Drop Oscillations in Electrowetting,” *Langmuir*, vol. 23, no. 9, pp. 5173–5179, Apr. 2007.

[26] W. Y. Lim, O. D. Supekar, M. Zohrabi, J. T. Gopinath, and V. M. Bright, “Liquid Combination with High Refractive Index Contrast and Fast Scanning Speeds for Electrowetting Adaptive Optics,” *Langmuir*, vol. 34, no. 48, pp. 14511–14518, Dec. 2018.

[27] O. D. Supekar, M. Zohrabi, J. T. Gopinath, and V. M. Bright, “Enhanced Response Time of Electrowetting Lenses with Shaped Input Voltage Functions,” *Langmuir*, vol. 33, no. 19, pp. 4863–4869, May 2017.

[28] E. J. Miscles, W. Y. Lim, O. D. Supekar, M. Zohrabi, J. T. Gopinath, and V. M. Bright, “Axisymmetrical resonance modes in an electrowetting optical lens,” *Appl. Phys. Lett.*, vol. 122, no. 20, p. 201106, May 2023.

[29] S. Terrab, A. M. Watson, C. Roath, J. T. Gopinath, and V. M. Bright, “Adaptive electrowetting lens-prism element,” *Opt. Express*, vol. 23, no. 20, p. 25838, Oct. 2015.

[30] M. Wang, Ed., *Lithography*. InTech, 2010.

[31] C. A. Rothenbach and M. C. Gupta, “High resolution, low cost laser lithography using a Blu-ray optical head assembly,” *Opt. Lasers Eng.*, vol. 50, no. 6, pp. 900–904, Jun. 2012.

[32] Y. K. Cheong, W. H. Lim, S. H. Lee, C. H. Pua, W. Y. Chong, and H. Ahmad, “405 nm laser processing of thin SU-8 polymer film,” *Optik*, vol. 127, no. 4, pp. 1651–1655, Feb. 2016.

[33] M. A. A. Neil, R. Juškaitis, and T. Wilson, “Method of obtaining optical sectioning by using structured light in a conventional microscope,” *Opt. Lett.*, vol. 22, no. 24, p. 1905, Dec. 1997.

[34] V. Kumar, K. Behrman, F. Speed, C. A. Saladrigas, O. Supekar, Z. Huang, V. M. Bright, C. G. Welle, D. Restrepo, J. T. Gopinath, E. A. Gibson, and I. Kymissis, “MicroLED light source for optical sectioning structured illumination microscopy,” *Opt. Express*, vol. 31, no. 10, p. 16709, May 2023.

[35] P. T. Brown, R. Kruithoff, G. J. Seedorf, and D. P. Shepherd, “Multicolor structured illumination microscopy and quantitative control of polychromatic light with a digital micromirror device,” *Biomed. Opt. Express*, vol. 12, no. 6, p. 3700, Jun. 2021.

CONTACT

*E.J. Miscles; Eduardo.Miscles@colorado.edu